Aquatic Toxicology 130–131 (2013) 123–131

Contents lists available at SciVerse ScienceDirect

Aquatic Toxicology

journal homepage: www.elsevier.com/locate/aquatox

Quantitative proteomic analysis reveals the mode-of-action for chronic mercury hepatotoxicity to marine medaka (*Oryzias melastigma*)

Minghua Wang, Yuyu Wang, Ling Zhang, Juan Wang, Huasheng Hong, Dazhi Wang*

State Key Laboratory of Marine Environmental Science/College of the Environment and Ecology, Xiamen University, Xiamen 361005, China

ARTICLE INFO

Article history:
Received 24 September 2012
Received in revised form 16 January 2013
Accepted 18 January 2013

Keywords:
Chronic mercury hepatotoxicity
Marine medaka
Quantitative proteomics
Two-dimensional difference gel electrophoresis

ABSTRACT

Mercury (Hg) is a widespread persistent pollutant in aquatic ecosystems. We investigated the protein profiles of medaka (*Oryzias melastigma*) liver chronically exposed to different mercuric chloride ($HgCl_2$) concentrations (1 or 10 μg/L) for 60 d using two-dimensional difference gel electrophoresis (2D-DIGE), as well as cell ultrastructure and Hg content analysis of the hepatic tissue. The results showed that Hg exposure significantly increased metal accumulation in the liver, and subsequently damaged liver ultrastructure. Comparison of the 2D-DIGE protein profiles of the exposed and control groups revealed that the abundance of 45 protein spots was remarkably altered in response to Hg treatment. The altered spots were subjected to matrix-assisted laser desorption/ionization tandem time-of-flight mass spectrometry analysis, with the resultant identification of 33 spots. These proteins were mainly involved in cytoskeleton assembly, oxidative stress, and energy production. Among them, several proteins related to mitochondrial function (e.g. respiratory metabolism) were significantly altered in the treated hepatocytes, implying that this organelle might be the primary target for Hg attack in the cells. This study provided new insights into the molecular mechanisms and/or toxic pathways by which chronic Hg hepatotoxicity affects aquatic organisms, and also provided basic information for screening potential biomarkers for aquatic Hg monitoring.

1. Introduction

The presence of industrial contaminants in the aquatic environment has been of increasing concern for human and wildlife health. Mercury (Hg) is of particular concern because of the bioaccumulation and potent neurotoxicity of some of its forms (Crump and Trudeau, 2009). Hg pollution, which is mainly attributable to anthropogenic activities including industrialization, has resulted in several catastrophic Hg poisoning events in Japan (Kudo et al., 1998), the Amazon Basin (Pfeiffer and Lacerda, 1988) and Iraq (Bakir et al., 1973). Recently, many high-risk sites with Hg pollution have been reported in Asia, since this area has become the largest contributor of anthropogenic atmospheric Hg, and is responsible for over half of the global emission (Li et al., 2009). Moreover, Hg pollution and poisoning have imposed a huge economic cost on environmental remediation and public health (Ung et al., 2010).

Several forms of Hg are present in the environment, including elemental, organic or inorganic (Morel et al., 1998), and all forms of Hg are very toxic and possible human carcinogens (ATSDR, 1999). The potent toxicity of Hg compounds is often associated with the high affinity of Hg for sulfur, causing an efficient biding to cysteine residues in proteins and enzymes, thereby perturbing their functions (Sørmo et al., 2011). Although Hg could produce multi-toxicities in organisms, most attention has been paid to Hg neurotoxicity and nephrotoxicity (Berg et al., 2010; Castoldi et al., 2001; Dieguez-Acuña et al., 2001; Keyvanshokooh et al., 2009; Nøstbakken et al., 2012; Torres et al., 2011). Consequently, there have been several molecular mechanistic studies on neurological (Castoldi et al., 2001) and renal (Zalups, 2000) toxicities induced by this metal. However, regardless of the occurrence of extensive biliary-hepatic cycling of Hg (Dutczak and Ballatori, 1994) and of some evidence suggesting that the liver plays a role in renal tubular uptake of Hg (Zalups, 2000), little is known about the mechanism of Hg-induced hepatotoxicity in organisms. Based on the role of liver function in Hg transformation and cycling, as well as its central role in the control and synthesis of critical blood constituents which affect the whole body physiology (Ung et al., 2010), it is postulated that Hg exposure could cause liver damage that might beget other syndromes. In fact, the above hypothesis is recently evidenced by a report in which Hg is clearly regarded as a cause of fulminant hepatic failure in a child (Al-Sinani et al., 2011). Thus, due to the prevalence of Hg exposure to humans, elucidation of the mode-of-action of Hg hepatotoxicity is very important to understand its impact on liver health.

* Corresponding author at: College of the Environment and Ecology, Xiamen University, Xiamen 361005, China. Tel.: +86 592 2186016; fax: +86 592 2180655.
E-mail address: dzwang@xmu.edu.cn (D. Wang).

0166-445X/$ – see front matter © 2013 Elsevier B.V. All rights reserved.
http://dx.doi.org/10.1016/j.aquatox.2013.01.012

"Omics" technologies such as genomics and proteomics have enabled simultaneous assessment of the expression profiles of hundreds and/or thousands of genes/proteins, and are intended to detect critical genes/proteins and pathways disrupted by exposure to harmful chemicals and environmental stressors (Merrick, 2006; Ung et al., 2010). Recently omics-based approaches have been applied well to investigate the mechanisms of Hg toxicity in fishes (Berg et al., 2010; Keyvanshokooh et al., 2009; Ung et al., 2010; Wang et al., 2011). Hg hepatotoxicity can induce oxidative stress, which is subsequently followed or accompanied by several toxic events, e.g. cytoskeletonal disruption, signal transduction dysregulation, and metabolic disorders (Ung et al., 2010; Wang et al., 2011). Nevertheless, most previous studies solely focused on acute Hg toxicity, although chronic exposure to low levels of Hg might be the main accumulation pathway for animals, including human beings, in the environment (Kim et al., 2005). In our study, medaka (*Oryzias melastigma*) were chronically exposed to different mercuric chloride ($HgCl_2$) concentrations (1 or 10 μg/L) for 60 d, and the protein profiles of the liver cells of exposed and non-exposed medaka were analyzed using two-dimensional difference gel electrophoresis (2D-DIGE), and the differentially expressed protein spots were identified using matrix-assisted laser desorption/ionization tandem time-of-flight mass spectrometry (MALDI-TOF/TOF MS) analysis. In addition, cell ultrastructure and total-mercury (T-Hg) content of the hepatic tissue were also examined. The purpose of this experiment was to elucidate the mode-of-action for chronic Hg hepatotoxicity in the medaka liver, and to provide scientific information for early warning of environmental health risk of Hg pollution.

2. Materials and methods

2.1. Medaka exposure experiment

Medaka (*O. melastigma*) were acclimatized in aerated seawater tanks for 15 d prior to the experiment at a water temperature of 25 °C under a 12 h light/dark cycle, and fed twice a day, 9:00 am and 3: 00 pm, with commercial artemia dry bait. Then, fish (each weighing 0.5 ± 0.05 g) were randomly assigned to three experimental groups for exposure to two Hg treatments, 1 and 10 μg/L, and non-exposure. Each treatment included two groups with 40 fishes in each group. The experiments were carried out in glass tanks (44 cm × 30 cm × 28 cm) with 30 L filtered seawater and lasted for 60 d under the same conditions as during acclimation, described above. Each day half of the aged seawater was renewed with fresh seawater containing 1 or 10 μg/L $HgCl_2$, or none. No mortality was found in the control and 1 μg/L-treated groups, but 5% mortality rate was observed in the 10 μg/L treatment. After the exposure, 24 medaka fish (12 per tank) from each treatment were collected together and then 8 of them were randomly selected for dissecting livers which were pooled together for proteomic analysis, hence producing three independent replicates for each treatment. Meanwhile, 36 medaka fishes (18 per tank) from each treatment were collected together and 12 of them were randomly selected for dissecting livers which were pooled together for Hg concentration analysis, with producing three replicates for each treatment. The remaining carcasses (at least 16 in each treatment) were dissected for livers which were subsequently fixed in 2.5% glutaraldehyde for cell ultrastructure analysis. It should be noted that the medaka used in this study were mixed-sex adult fish of the same age. All seawater used was filtered through 0.45 μm acetate fiber membranes, with the background concentration of T-Hg being 0.0051 μg/L. The seawater characteristics were described as follows: dissolved oxygen, 6.2–6.7 mg/L; salinity, 29–30 PSU; and pH 8.0–8.1.

2.2. Hg concentration analysis

T-Hg concentrations in the livers were measured using the EPA 7474 method. Briefly, after freeze-drying for 2 d, the tissues were digested in 70% nitric acid in a heating block at 80 °C overnight and, in the hydrochloride/bromate/bromide mixture (Sigma, USA), the Hg was oxidized with stannous chloride (Wako) and analyzed using cold vapor atomic fluorescence spectrometry (CVAFS, Brooks Rand Model III) (Pan and Wang, 2011). A certified reference material (Mussel homogenate IAEA 142) was concurrently digested and measured for T-Hg, and the recovery rate was >90% in the standard. T-Hg content in medaka livers was measured as ng/g dry weight (DW), and the data were expressed as mean values ± standard deviation (SD).

2.3. Ultrastructure analysis

Fish livers were fixed in 2.5% glutaradehyde in 0.1 M phosphate buffer (pH 7.3) for 3 h at 4 °C. The fixed livers were washed three times using 0.1 M phosphate buffer (pH 7.3) at 20 min intervals with periodic agitation, then further fixed in 1% osmium tetroxide for 2 h at 4 °C, followed by a phosphate buffer wash three times at 20 min intervals. After dehydration in alcohol, the livers were embedded in Epon-Araldite. Ultra-thin sections (50–80 nm) were moved onto titanium grids, stained with uranyl acetate and lead citrate and observed using a JEM 2100 Transmission Electron Microscope. Image analysis was conducted using the ImageJ 1.36 program (NIH, Washington, DC).

2.4. Proteomic analysis

2.4.1. Protein extraction

Proteins were extracted from medaka livers according to the trichloroacetic acid (TCA)/acetone precipitation method introduced by Görg et al. (1997) with minor modification. Briefly, frozen fish livers were suspended in 1 mL of 10% w/v trichloroacetic acid (TCA)/acetone for 1 h at 4 °C. After centrifugation at 18,000 × *g* for 30 min at 4 °C, the pellets were recovered and subsequently homogenized in 1.0 mL of 20% TCA/acetone (w/v) lysis buffer using an ultrasonic disrupter. The supernatant was removed by centrifugation at 18,000 × *g* for 30 min at 4 °C, and the pellet was washed twice with 80% acetone (v/v) and twice with ice-cold acetone. The pellet was recovered by centrifugation at 18,000 × *g* for 30 min at 4 °C each time. Residual acetone was removed in a SpeedVac for about 5 min. The pellet was dissolved in 120 μL rehydration buffer containing 30 mM Tris, 7 M urea, 2 M thiourea, and 4% CHAPS (Bio-Rad, USA). The solution was centrifuged at 20,000 × *g* for 30 min at 10 °C and the supernatant was collected for 2D-DIGE analysis. Protein concentrations were quantified using the 2-D Quant kit (GE Healthcare, USA).

2.4.2. CyDye labeling

The proteins were labeled with CyDyes for performing 2D-DIGE analysis (Wang et al., 2012). Prior to protein labeling, the pH of the samples was checked with a pH indicator strip, and if necessary the pH was adjusted to 8.5 using 50 mM NaOH. An internal standard was prepared by making a mixture with equal amounts of all the samples used in this experiment. The protein samples were labeled with Cy3 or Cy5 cyanine dye and the internal standard with Cy2 dye, by adding 400 pmol of CyDye per 50 μg protein. The labeling reaction was performed for 30 min on ice in the dark. Afterward, the reaction was quenched with the addition of 1 μL 10 mM L-lysine (Sigma, USA) followed by incubation for 10 min on ice in the dark.

2.4.3. 2D-DIGE analysis

After labeling, the samples were combined according to the dye-swapping scheme (Table S1, Supplementary material). In total, nine samples were obtained in this study (three replicates per group), and the samples were run in five gels. The combined mixtures containing 150 μg protein were brought up to a final volume of 450 μL with 1× rehydration buffer, after which 0.5% IPG buffer 4–7 (GE Healthcare, USA) was added and they were mixed thoroughly. The labeled samples were then applied to the strips on an Ettan IPGphor III Isoelectric Focusing System (GE Healthcare, USA). Isoelectric focusing was conducted for a total of 60 kV-h using the following conditions: 40 V for 5 h, 100 V for 6 h, gradient to 500 V in 30 min, gradient to 1000 V in 30 min, gradient to 2000 V in 1 h, gradient to 10,000 V in 1 h, and finally 10,000 V for 6 h. After the first dimension was run, each strip was equilibrated with about 10 mL equilibration buffer containing 50 mM Tris (pH 8.8), 6 M urea, 30% glycerol, 2% SDS, 1% DTT and a trace amount of bromophenol blue, for 17 min. The strip was then placed in fresh equilibration buffer containing 2.5% iodoacetamide (instead of DTT) for another 17 min. Subsequently an 11.5% SDS-PAGE second dimension was performed. Electrophoresis was carried out at 10 mA/gel for 15 min, followed by a 6 h run at 200 V until the bromophenol blue front reached the edge of the gels. The protein spot patterns of the three different dyes were acquired using an Ettan DIGE Imager laser scanner (GE Healthcare, USA) at excitation/emission wavelengths of 488/520 nm (Cy2), 532/670 nm (Cy3), and 633/670 nm (Cy5). The exposure time of the laser was chosen in such a way that the protein spots had no saturated signal. After imaging for CyDye, the gels were further subjected to silver staining.

2.4.4. Data analysis

Image analysis was performed using the DeCyder version 6.5 suite (GE Healthcare, USA). First, protein spot detection and quantification compared with the internal standard as a volume ratio was performed with the Differential In-gel Analysis module. Second, protein spots on different gels were matched, and statistical analysis was carried out with the Biological Variation Analysis module. One-way ANOVA ($P < 0.05$) was used to pick out the significant differential protein spots among the groups. When the spots were selected as significant, they were carefully checked for correct matching throughout all the gels and were included in the pick list. Then, the fold changes of treatment/control were calculated based on differences in their standardized abundance.

2.4.5. Silver staining

Silver staining was performed following the method (Wang et al., 2010). Briefly, the gel was initially fixed for 2 h in a fixation solution containing 40% (v/v) ethanol and 10% (v/v) acetic acid. It was then sensitized in a solution containing 30% (v/v) ethanol, 0.2% (w/v) sodium thiosulphate, 6.8% (w/v) sodium acetate and 0.125% (v/v) glutaraldehyde, followed by three Milli-Q water washes (5 min each time). Then the gel was stained for 20 min in 0.25% (w/v) silver nitrate with 0.015% (v/v) formaldehyde and washed twice with Milli-Q water (0.5 min each time). The gel was developed in 2.5% (w/v) sodium carbonate containing 0.0074% (v/v) formaldehyde. The reaction was stopped with 1.5% (w/v) ethylenediaminetetraacetic acid, disodium salt.

2.5. Mass spectrometric analysis

The altered protein spots were manually excised from 2-DE gels. The gel pieces were washed with buffer containing 25 mM ammonium bicarbonate in 50% acetonitrile (ACN), destained with 30 mM potassium ferricyanide and 100 mM sodium thiosulfate, and washed again with 25 mM ammonium bicarbonate in 50% ACN. After dehydration with 100% ACN, the dry gel pieces were digested by adding 10.0 ng/μL trypsin (Promega, Madison, WI) in 25 mM ammonium bicarbonate overnight at 37 °C. For MALDI-TOF/TOF MS analysis, 1 μL of the digest mixture was mixed with 0.5 μL of 100 mM α-cyano-4-hydroxy-cinnamic acid in 50% ACN/0.1% trifluoroacetic acid on the target plate before being dried and analyzed with a MALDI-TOF/TOF mass spectrometer (5800 Proteomics Analyzer, Applied Biosystems, Foster City, CA). MALDI-TOF MS and TOF-TOF tandem MS were performed and data were acquired in the positive MS reflector mode with a scan range from 900 to 4000 Da, and five monoisotopic precursors (S/N > 200) were selected for MS/MS analysis. For interpretation of the mass spectra, a combination of peptide mass fingerprints and peptide fragmentation patterns were used for protein identification in an NCBI nonredundant database against all entries using the Mascot search engine (www.matrixscience.com). All mass values were considered monoisotopic, and peptide tolerance was 75 ppm and 0.3 Da for MS and MS/MS spectra, respectively. One missed cleavage site was allowed for trypsin digestion; cysteine carbamidomethylation was assumed as a fixed modification, and methionine was assumed to be partially oxidized. Results with C.I.% (Confidence Interval%) values greater than 95% were considered to be a positive identification. The identified proteins were then matched to specific processes or functions by searching Gene Ontology (http://www.geneontology.org/).

2.6. Network analysis

The differentially expressed proteins were further analyzed for their association with network pathways using MetaCore from GeneGo Inc., an integrated manually curated knowledge database for pathway analysis of genes lists (http://www.genego.com/metacore.php). MetaCore consists of curated protein interaction networks on the basis of manually annotated and regularly updated database. For each identified protein, the appropriate human homologue was obtained in the UniProtKB/Swiss-Prot database using the online Protein Identifier Cross-Reference Service (http://www.ebi.ac.uk/Tools/picr/search.do). Subsequently, the homologues for medaka proteins were then uploaded into the GeneGo environment. Hypothetical networks of proteins from our experiment and proteins from the MetaCore database were then built using the shortest paths algorithm.

2.7. Statistical tests

All measurements were replicated at least three times and the data were expressed as mean values ± SD. Statistical analysis was carried out using a one-way ANOVA or an independent-samples *t*-test to evaluate whether the means were significantly different among the groups. Significant differences were indicated at $P < 0.05$. Prior to one-way ANOVA, data were log transformed to meet ANOVA assumptions of normality and variance homoscedasticity.

3. Results

3.1. Hg accumulation in medaka liver

After the exposure, the medaka livers were subjected to T-Hg content analysis. T-Hg concentration in the control livers was 90.3 ± 19.6 ng/g DW, whereas Hg treatment significantly enhanced T-Hg accumulation in the treated livers (Fig. 1, $P < 0.001$), i.e. the T-Hg contents were 13,013.3 ± 1430.8 and 76,467.7 ± 8617.6 ng/g DW in the livers exposed to 1 and 10 μg/L $HgCl_2$, respectively.

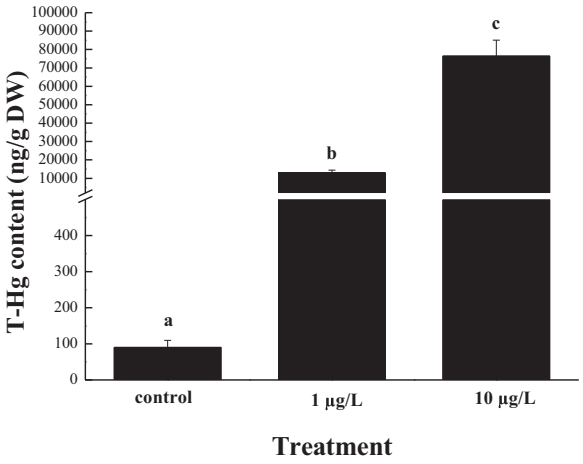

Fig. 1. Total-mercury (T-Hg) contents in the hepatic tissue of the medaka *Oryzias melastigma* after 60 d exposure to different mercury chloride concentrations (control, 1 and 10 μg/L). Data are expressed as mean values ± SD ($n = 3$). Different letters indicate a statistically significant difference at $P < 0.05$.

3.2. Effects of Hg on liver ultrastructure in medaka

Hepatocytes of control medaka contained few cisternae in the rough endoplasmic reticulum (ER), which were presented in parallel layers or tightly associated with the mitochondria. Nucleoli were located in the center of the spherically shaped nuclei, the nucleoplasm exhibited very little heterochromatin, and the nucleolus displayed electron density. Meanwhile, glycogen was evenly distributed in the cytoplasm (Fig. 2A). After 60 d exposure, a widespread swelling was observed in the rough ER, with dilation or even vesiculation of the cisternae, especially in the medaka livers exposed to 10 μg/L $HgCl_2$ treatment. A dose-dependent swelling of the mitochondria was observed in the Hg-treated hepatocytes which did not present cristae. Dilation of the nuclear envelope was also observed in the 10 μg/L Hg treatment.

3.3. $HgCl_2$-induced proteome alterations

A representative 2D-DIGE image is shown in Figure S1 (Supplementary material). In all, approximately 2000 spots could be matched with all the images. Out of these matched spots, 45 significantly differential spots were detected with a one-way ANOVA test ($P < 0.05$ with differences of ≥1.5 in expression), and all of them were submitted for MALDI-TOF/TOF MS analysis. Among them, 33 protein spots were successfully identified with C.I.% values greater than 95%, and all the matched proteins came from the NCBI database for fish species (Table 1). Of them, four protein spots (spots 4, 7, 8 and 34) were involved in cytoskeletonal assembly. Seven (spots 9, 17, 19, 20, 36, 43 and 44) were correlated with oxidative stress, and all of them were consistently up-regulated in abundance under Hg treatment. Three protein spots (spots 26, 30 and 41) played a role in respiratory metabolism, and their expressions were significantly down-regulated in the 10 μg/L $HgCl_2$-treated group. Also, eight protein spots (spots 10, 13, 15, 25, 27, 28, 31 and 32) were related to other types of metabolism (e.g. carbohydrate and fatty acid metabolism). Meanwhile, 11 protein spots

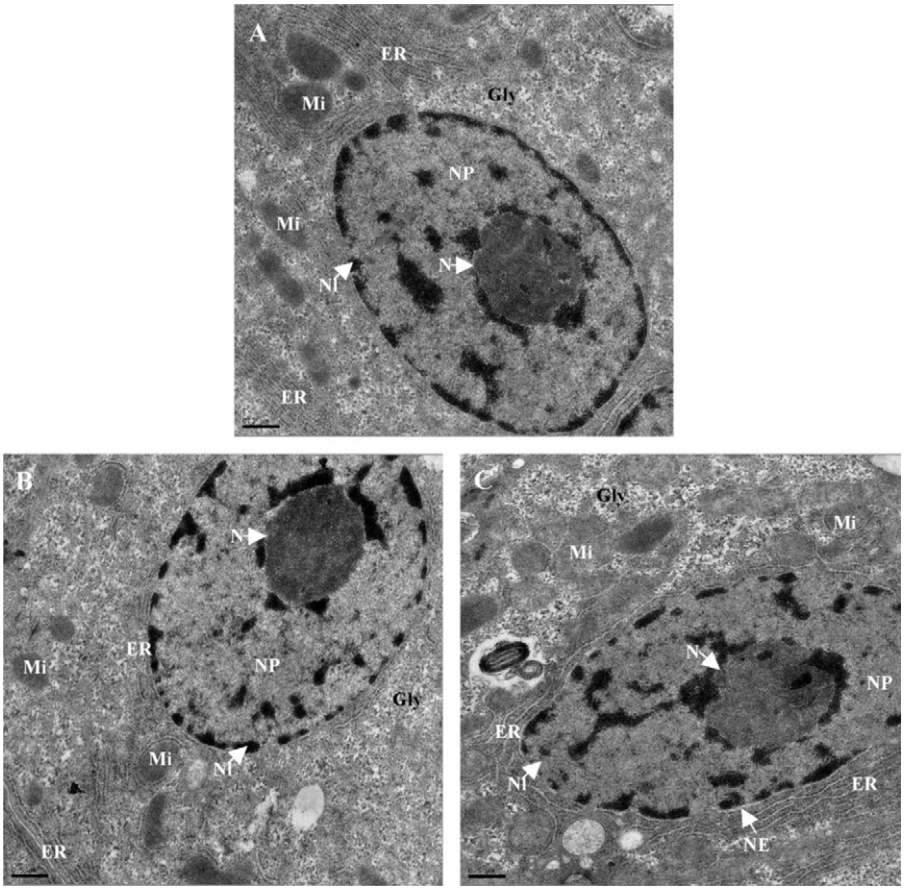

Fig. 2. Transmission electron micrographs of liver cells of the medaka *Oryzias melastigma* after 60 d exposure to different mercury chloride ($HgCl_2$) concentrations. (A) Control, (B) 1 μg/L $HgCl_2$, and (C) 10 μg/L $HgCl_2$. Marked features are: ER, endoplasmic reticulum; Gly, glycogen; Mi, mitochondria; N, nucleolus; NE, nuclear envelop; Nl, nucleus; NP, nucleoplasm.

Table 1
A detailed list of protein spots identified using MALDI-TOF/TOF MS from the liver of medaka *Oryzias melastigma* following $HgCl_2$ exposure.

Spot id.	Protein identity [Gene names]	Accession number	MASCOT score (peptides)	Protein score C.I.%	MW/p*I*	Organism	Molecular function	Fold change	
								1 μg/L	10 μg/L
Cytoskeletonal assembly									
4	Keratin 15 [krt15]	gi|28278622	83 (12)	99.92	49.12/5.13	*Danio rerio*	Structural molecule activity	−2.69	–
7	Type I cytokeratin, enveloping layer [cyt1]	gi|18858519	147 (11)	100	46.66/5.13	*Danio rerio*	Structural molecule activity	1.70	–
8	Keratin K10 [krt10]	gi|119709407	71 (7)	98.74	44.63/4.88	*Lepisosteus oculatus*	Structural molecule activity	1.59	–
34	Novel protein similar to vertebrate plectin 1 [PLEC]	gi|153792369	66 (48)	96.01	52.41/6.29	*Danio rerio*	Actin binding	–	−3.84
Oxidative stress									
9	Cathepsin D [ctsd]	gi|157644743	103 (2)	100	43.45/5.80	*Lates calcarifer*	Aspartic-type endopeptidase activity	1.92	2.62
17	Glutathione S-transferase [gstR]	gi|110180509	75 (1)	99.54	8.07/5.42	*Oryzias javanicus*	Transferase activity	1.56	2.07
19	DJ-1 protein [dj-1]	gi|157278183	108 (5)	100	20.03/6.10	*Oryzias latipes*	Unknown	1.53	1.66
20	Peroxiredoxin-1 [PRDX1]	gi|229366138	66 (4)	96.29	22.20/6.30	*Anoplopoma fimbria*	Antioxidant activity	2.01	2.95
36	Natural killer enhancing factor	gi|93211500	167 (3)	100	22.06/5.58	*Psetta maxima*	Antioxidant activity	–	17.74
43	Glutathione S-transferase	gi|183604400	61(2)	99.72	26.03/8.24	*Channa maculata*	Transferase activity	–	1.55
44	Peroxiredoxin-2 [PRDX2]	gi|50539996	107 (2)	100	21.91/5.93	*Danio rerio*	Antioxidant activity	–	5.59
Respiratory metabolism									
26	ATP synthase subunit d, mitochondrial [ATP5H]	gi|225717172	60 (3)	98.92	18.21/5.55	*Esox lucius*	Transporter activity	–	−1.60
30	Electron-transferring-flavoprotein dehydrogenase [etfdh]	gi|52219050	82 (4)	99.90	69.51/6.75	*Danio rerio*	Electron carrier activity	–	−1.81
41	Electron transferring flavoprotein subunit alpha, mitochondrial [ETFA]	gi|225707506	109 (3)	100	35.45/7.01	*Osmerus mordax*	Electron carrier activity	–	−1.54
Other metabolism									
10	Pyruvate dehydrogenase (lipoamide) beta [pdhb]	gi|47085923	90 (2)	99.99	39.63/5.78	*Danio rerio*	Pyruvate dehydrogenase activity	1.60	–
13	Phytanoyl-CoA dioxygenase domain-containing protein 1 [PHYD1]	gi|55925379	95 (3)	100	33.40/5.39	*Danio rerio*	Oxidoreductase activity	1.99	–
15	Delta3,5-delta2,4-dienoyl-CoA isomerase, mitochondrial [ECH1]	gi|225706936	144 (3)	100	33.54/6.54	*Osmerus mordax*	Isomerase activity	1.81	–
25	Phosphorylase [pygb]	gi|67810298	242 (17)	100	98.36/6.84	*Oreochromis mossambicus*	Phosphorylase activity	–	−1.71
27	Phosphorylase [pygb]	gi|67810298	209 (13)	100	98.36/6.84	*Oreochromis mossambicus*	Phosphorylase activity	–	−1.86
28	Phosphorylase [pygb]	gi|67810298	91 (19)	99.99	98.36/6.84	*Oreochromis mossambicus*	Phosphorylase activity	–	−1.79
31	Formimidoyltransferase-cyclodeaminase [FTCD]	gi|259155104	66 (8)	98.65	59.93/5.70	*Salmo salar*	Folic acid binding	–	−2.85
32	Formimidoyltransferase-cyclodeaminase [FTCD]	gi|259155104	64 (7)	95.46	59.93/5.70	*Salmo salar*	Folic acid binding	–	4.23
Other functions related									
33	Eukaryotic translation initiation factor 3, subunit 2 beta [eIF3S2]	gi|55742565	119 (4)	100	36.72/5.22	*Danio rerio*	Nucleic acid binding	–	−1.92
38	Histone H4	gi|115495857	87 (5)	99.97	11.34/11.4	*Danio rerio*	DNA binding	–	1.65
39	Ependymin [epd]	gi|156106236	63 (1)	97.50	24.24/5.25	*Perca flavescens*	Calcium ion binding	–	4.68
40	GammaN1 crystallin [CRYGN1]	gi|222522583	127 (7)	100	21.95/5.97	*Poecilia reticulata*	Unknown	–	1.68
1	Unnamed protein product	gi|47211167	68 (3)	97.31	55.07/8.10	*Tetraodon nigroviridis*	Unknown	1.69	–
2	Unnamed protein product	gi|47215577	96 (5)	100	102.45/6.0	*Tetraodon nigroviridis*	Unknown	1.82	–
6	Unnamed protein product	gi|47223261	67 (1)	96.61	21.34/5.49	*Tetraodon nigroviridis*	Unknown	2.47	–
21	Unnamed protein product	gi|47223289	67 (16)	97.05	99.53/9.48	*Tetraodon nigroviridi*	Unknown	5.19	6.09
22	Unnamed protein product	gi|47229947	71 (4)	98.78	14.92/6.59	*Tetraodon nigroviridi*	Unknown	2.81	–
24	Unnamed protein product	gi|47228715	68 (2)	97.25	18.34/5.29	*Tetraodon nigroviridi*	Unknown	1.52	–
29	Unnamed protein product	gi|47204593	100 (2)	100	71.06/6.01	*Tetraodon nigroviridi*	Unknown	–	1.60

Note: MW represents molecular weight with p*I* for isoelectric point. Variations were calculated as treated/control spot volume ratio and if the result was below 1, it is reported as – control/treated ratio.

(spots 33, 38, 39, 40, 1, 2, 6, 21, 22, 24 and 29) were correlated with other functions. For example, spots 33 and 38 were involved in protein translation, and spot 39 in signal transduction. It should be emphasized that several protein spots were identified as the same protein in this experiment, e.g. spots 17 and 43 for glutathione S-transferase (GST), spots 25, 27 and 28 for phosphorylase, and spots 28 and 31 for formimidoyltransferase-cyclodeaminase. These protein spots might be protein isoforms, which can arise from alternative mRNA splicing and various post-translational modifications, such as cleavage, phosphorylation, acetylation and glycosylation.

3.4. Protein interaction network analysis

Using the network building tool MetaCore, a top scored network pathway was built from the differentially identified proteins in this experiment. Six proteins (Plectin 1, PRDX1, ATP5H, PDH beta, eIF3S2 and ETFA) were involved in this pathway, which was mainly correlated with response to stress and wound healing (Fig. 3). Individual proteins are represented as nodes. This pathway could be classified as the c-myc pathway, since the root nodes were connected to c-myc directly or indirectly, and their expression levels or activities could be regulated by c-myc. In addition, some of them (e.g. PRDX1) could regulate c-myc activity in a feedback manner.

4. Discussion

Many studies have been devoted to Hg toxicity in various aquatic organisms. Our study, to our best knowledge, was the first effort to investigate the mode-of-action of chronic Hg hepatotoxicity in organisms at the proteomic level. Our results showed that chronic exposure to 1 and 10 μg/L Hg significantly increased metal concentrations in the medaka liver, which is consistent with a previous study that Hg accumulates in several tissues including the liver of the fish *Brycon amazonicus* after $HgCl_2$ treatment (Monteiro et al., 2010). Hg accumulation in our experiment was comparable with the metal content in the medaka liver after an acute exposure of 8 h to 1000 μg/L $HgCl_2$ treatment in our previous work (Wang et al., 2011), highlighting that chronic exposure to lower levels of Hg leads to a rapid hepatic accumulation. Meanwhile, T-Hg contents in the Hg-exposed livers in our study were within the span of Hg concentrations in several fish species in the environment (Cardellichio et al., 2002; Frodello et al., 2000), hence enabling this study to show an environmentally related significance.

Our study showed that chronic Hg toxicity caused damage to liver ultrastructure in medaka. Damage to hepatocytes following in vivo treatment with Hg is reported (Giari et al., 2008; Ung et al., 2010). Hepatocytes of *Dicentrarchus labrax* present dilated cisternae of the rough ER, swelling of mitochondria, cristae regression, changes to the electron-transparency of the matrix in the treated fishes, and dilation of the nuclear envelope with an accumulation of heterochromatin in the highest treatment (Giari et al., 2008). Similarly, Ung et al. (2010) report that $HgCl_2$ treatment has caused morphological changes of liver parenchyma, reduced nucleated cells and increased lipid vesicles, glycogen and apoptotic bodies in zebrafish. Overall, these results demonstrate that Hg causes a significant disruption of cytoskeleton organization in the hepatocytes.

Our proteomic analysis clearly demonstrated that chronic Hg toxicity caused oxidative stress to medaka liver, since seven protein spots involved in cellular redox maintenance were up-regulated after metal exposure. Cathepsin D is a lysosomal aspartic protease and its primary biological function is protein degradation in the acidic milieu of lysosomes. Cathepsin D is a mediator of apoptosis and is induced by several stimuli including oxidative stress (Beaujouin et al., 2006; Kagedal et al., 2001; Sheikh et al., 2010). In this study, the up-regulation of cathepsin D in medaka livers indicated that Hg exposure might enhance cells to synthesize more cathepsin D to degrade cellular damaged proteins caused by Hg toxicity. Directly related to oxidative stress response is the increased expression of GST, an enzyme that catalyzes the conjugation of glutathione of a large variety of electrophilic compounds, including products resulting from oxidative damage in biological membranes and macromolecules (Hayes and McLellan, 1999). Peroxiredoxins also play a physiologically important role in the enzymatic removal of reactive oxygen species (ROS) (Radyuk et al., 2001). Natural killer enhancing factor belongs to a highly conserved peroxiredoxin family, and its functions are involved in immune cytotoxicity, apoptostis, cell proliferation, differentiation and antioxidative activity (Dong et al., 2007). In our experiment, the overexpression of GST, peroxiredoxin-1, peroxiredoxin-2 and natural killer enhancing factor in the Hg-treated liver indicated a biological response aimed at reducing Hg toxic effects, and thus avoiding oxidative damage, since Hg exerts its toxicity at least in part through the induction of ROS by binding to intracellular thiols and acting as a catalyst in Fenton-type reactions (Stacchiotti et al., 2009). Noticeably, DJ-1 protein was found to be strikingly up-regulated in abundance after 10 μg/L Hg treatment. DJ-1 protein is responsible for the onset of familial Parkinson's disease, PARK7 (Bonifati et al., 2003). However, DJ-1 protein also displays anti-oxidative functions, serves as a chaperone and has protease activities involved with mitochondrial regulation (Cookson, 2003). Specifically, knockdown to the Japanese medaka homolog of human DJ-1 protein renders cultured medaka OLHE-13 cells susceptible to H_2O_2-induced cell death, which clearly suggests a protective role of DJ-1 protein against oxidative stress (Li et al., 2006).

Cytoskeleton disruption is a primary response of the cells to Hg toxicity (Wang et al., 2011). Keratins are important intermediate filament proteins, and their primary function is to protect cells from stress damage which may result in cell death, and to maintain normal signal transduction (Looi et al., 2009; Schaffeld and Schultess, 2006). The alteration of several keratins by Hg toxicity suggested an effect on tissue integrity. Also, the 10 μg/L concentration of Hg depressed the expression of a novel protein similar to vertebrate plectin 1. Plectin is a versatile cytolinker protein, which can bind to all major cytoskeleton filament networks and plays an important role as a mechanical linker and anchoring protein of intermediate filaments (Wiche, 1998). Consequently, the variations of cytoskeletal proteins indicated that Hg toxicity caused cellular damage in the hepatocytes due to cytoskeletal disruptions, and to some extent this was also highlighted by our ultrastructure study.

Our study showed that Hg might impair respiratory metabolism. Three proteins (ATP synthase subunit d, mitochondrial; electron-transferring-flavoprotein dehydrogenase; and electron transfer flavoprotein subunit alpha, mitochondrial) were diminished following the 10 μg/L Hg treatment. Mitochondrial ATP synthase is involved in ATP synthesis (Leyva et al., 2003). Electron-transferring-flavoprotein dehydrogenase is an enzyme that transfers electrons from electron transferring flavoprotein in the mitochondrial matrix, to the ubiquinone pool in the inner mitochondrial membrane (He et al., 2007). Decreased expression of the respiratory proteins might undermine the ability of the cells to meet their energy requirements and could therefore result in cellular damage and death. Carbohydrate metabolism (i.e. pyruvate dehydrogenase (lipoamide) beta and phosphorylase) (Ibarz et al., 2010; Samikkannu et al., 2003), and fatty acid oxidation (i.e. phytanoyl-CoA dioxygenase domain-containing protein 1, and delta3,5-delta2,4-dienoyl-CoA isomerase, mitochondrial) (McDonough et al., 2005; Newton et al., 2009) were also targets of Hg, and could impact cellular energy. Taken together, Hg toxicity caused impairment of energy generation and macromolecule

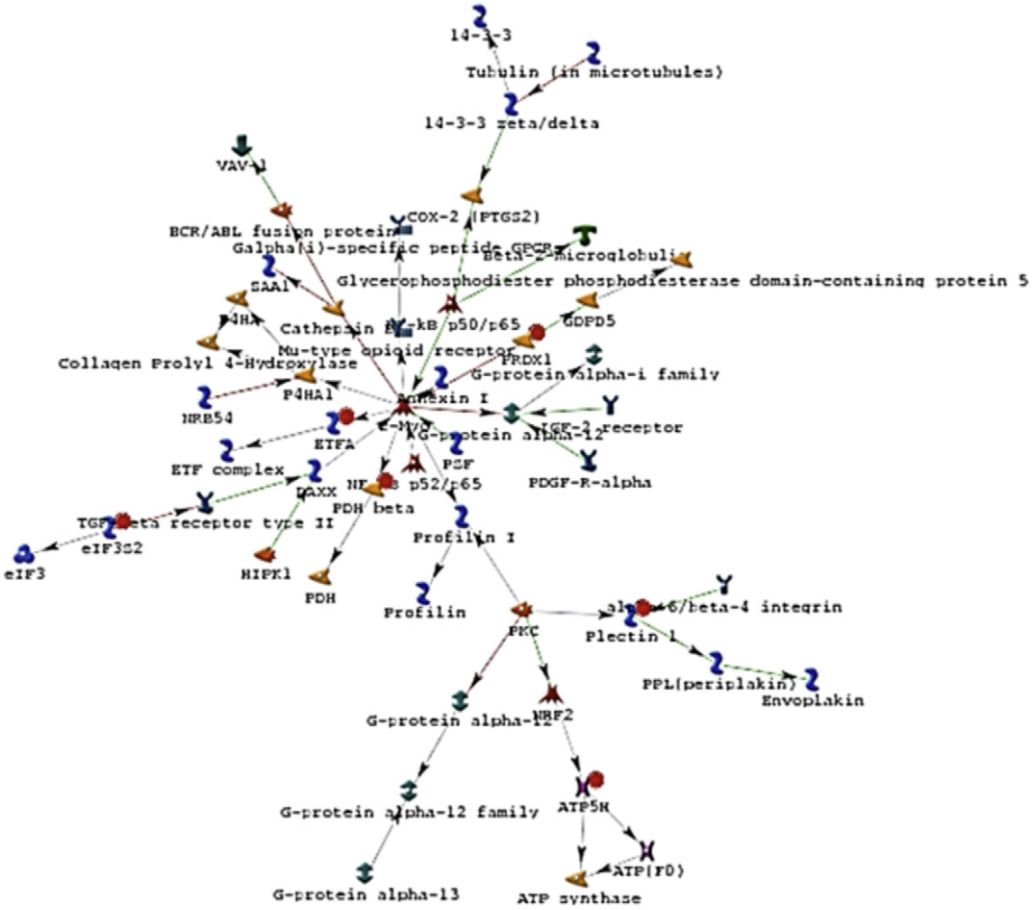

Fig. 3. Pathway analysis result shows that 6 differentially expressed proteins following mercury treatment could be sorted into the c-myc pathway. Individual proteins are represented as nodes, the different shapes of the nodes represent the functional class of the proteins, and the arrowheads indicate the direction of the interaction. Proteins marked with red circle represented the proteins identified from this study. ATP5H: ATP synthase subunit d, mitochondrial; c-myc: myelocytomatosis oncogene; eIF3S2: eukaryotic translation initiation factor 3, subunit 2 beta; ETFA: electron transferring flavoprotein subunit alpha, mitochondrial; NRF2: nuclear factor-erythroid 2-related factor 2; PDH beta: pyruvate dehydrogenase (lipoamide) beta; PKC: protein kinase C; Plectin 1: novel protein similar to vertebrate plectin 1; PRDX1: peroxiredoxin-1. (For interpretation of the references to color in this figure legend, the reader is referred to the web version of the article.)

metabolism, and eventually led to metabolic disorders that may cause further liver injury.

Eukaryotic translation initiation factor 3, subunit 2 beta (eIF3S2) was down-regulated by Hg. Reduced eIF3S2 is involved in apoptosis during metal toxicity (Shen et al., 2009), which suggests that Hg toxicity might lead to cell death due to metal-induced oxidative stress in the fish liver. Additionally, ependymin is increased by the highest Hg treatment. Ependymin is secreted by meningeal cells (Hoffmann, 1992), and is an important glycoprotein in the cerebrospinal fluid of teleost fish (Königstorfer et al., 1989). Interestingly, ependymin expression is induced in fish under environmental stress (Tang et al., 1999; Volz et al., 2006). For example, Volz et al. (2006) report that ependymin is highly induced after the day-1 transcriptional response in the highest dioxin treatment, suggesting that this gene may have been involved in host adaptation following hepatocyte injury.

A hypothetical network was built from the differentially expressed proteins of our experiments and proteins from the MetaCore database. The pathway analysis showed that six proteins of the identified differentially expressed spots were connected to c-myc in a complex signaling network via multiple modes, thus placing c-myc as one of the master factors involved in the mode-of-action of Hg hepatotoxicity. The c-myc protein is a transcription factor that plays an important role in cell death (e.g. apoptosis) but it is also involved in cell cycle progression and cellular transformation. A study shows that oxidative stress induces the expression of *c-fos*, *c-juc*, and *c-myc* in rat PTE cells (Maki et al., 1992). Meanwhile, Joseph et al. (2001) find that cadmium-induced overexpression of *c-myc* is mediated by the elevation of intracellular levels of ROS and calcium. Accordingly, we supposed that Hg treatment might have increased c-myc activity via induction of oxidative stress in our study; however, this deserves further examination. Another important node from this network was protein kinase C (PKC). Badou et al. (1997) show that $HgCl_2$ directly activates PKC and induces a PKC-dependent Ca^{2+} influx as a molecular target for $HgCl_2$. It should be noted that NRF2 (another node in this pathway) might be involved in the feedback process in response to Hg exposure. Toyama et al. (2007) find that NRF2 is a critical transcription factor in the reduction of Hg-induced cytotoxicity and the excretion of Hg into the extracellular space, because NRF2 deletion significantly enhances Hg accumulation and cytotoxicity in primary mouse hepatocytes. However, the exact interaction of Hg with the above signaling transduction components is not known and requires further investigation.

It should be emphasized that the proteomic response in the medaka liver was dependent on the ambient $HgCl_2$ concentrations. Of the 33 differentially expressed protein spots, 16 were observed in the 1 μg/L treatment and 22 were found in the 10 μg/L group, while only 5 were detected in both treatments (Table 1), indicating that the toxic mechanisms of low and high Hg concentrations were different. Proteins involved in cytoskeleton assembly and oxidative stress were significantly affected by low Hg concentration,

while proteins participating in respiratory metabolism, oxidative stress, phosphorylase activity, and binding activity were remarkably affected by high Hg concentration. Our ultrastructural result also revealed a dose-dependent swelling of the mitochondria in the Hg-treated hepatocytes. We also noted that the proteomic response in this study displayed some similarity with that in the medaka liver acutely exposed to $HgCl_2$ in our previous work (Wang et al., 2011), the major cellular processes affected by Hg were similar in terms of their general functional categories (e.g. cytoskeletonal assembly, oxidative stress, and energy metabolism). However, most of the individual proteins were significantly different, suggesting that the toxic mechanisms caused by acute or chronic Hg exposure were different. It is known that, in response to a toxicant exposure, the organisms would try to compensate for the loss/impairment of certain pathways caused by the toxicant at low doses via activation and deactivation of biochemical processes (adaptation processes), and subsequently, with the increase of toxicant concentration, the deregulation responses due to adverse irreversible damage may become predominant (Denslow et al., 2007; Gündel et al., 2012). Overall, our proteomic analysis revealed that the toxic mechanisms caused by inorganic Hg in medaka fish were related to the ambient Hg concentration and the manner of exposure.

5. Conclusions

This study showed that chronic Hg exposure significantly increased metal accumulation in Hg-treated medaka liver, and damaged liver ultrastructure. Quantitative proteomic analysis demonstrated that Hg hepatotoxicity might involve oxidative stress, cytoskeleton impairment and altered energy metabolism. Several proteins related to mitochondrial function (e.g. respiratory metabolism) were affected in the Hg-treated hepatocytes, highlighting that this organelle might be an important target for Hg attack. Also, some proteins in a dose-dependent response to Hg treatment (e.g. cathepsin D, GST and peroxiredoxin-1) could be used as potential biomarkers to aquatic Hg monitoring.

Acknowledgments

This work was supported by the National Natural Science Foundation of China (No. 40806051), the State Key Laboratory of Marine Environmental Science (Xiamen University), and the Program for New Century Excellent Talents in Universities of China to D.-Z. Wang. The authors appreciate the kind help of Dr. Wen-Xiong Wang and Ke Pan (The Hong Kong University of Science & Technology) in Hg analysis. Also, the authors thank Prof. John Hodgkiss for helping to revise the manuscript.

Appendix A. Supplementary data

Supplementary data associated with this article can be found, in the online version, at http://dx.doi.org/10.1016/j.aquatox.2013.01.012.

References

Al-Sinani, S., Al-Rawas, A., Dhawan, A., 2011. Mercury as a cause of fulminant hepatic failure in a child: case report and literature review. Clinics and Research in Hepatology and Gastroenterology 35 (8–9), 580–582.

ATSDR, 1999. Toxicological Profile for Mercury, Agency for Toxic Substances and Disease Registry, Atlanta, GA; U.S. Department of Health and Human Services, Public Health Service.

Badou, A., Savignac, M., Moreau, M., Leclerc, C., Pasquier, R., Druet, P., Pelletier, L., 1997. $HgCl_2$-induced interleukin-4 gene expression in T cells involves a protein kinase C-dependent calcium influx through L-type calcium channels. Journal of Biological Chemistry 272 (51), 32411–32418.

Bakir, F., Damluji, S.F., Amin-Zaki, L., Murtadha, M., Khalidi, A., Al-Rawi, N.Y., Tikriti, S., Dahahir, H.I., Clarkson, T.W., Smith, J.C., Doherty, R.A., 1973. Methylmercury poisoning in Iraq. Science 181 (4096), 230–241.

Beaujouin, M., Baghdiguian, S., Glondu-Lassis, M., Berchem, G., Liaudet-Coopman, E., 2006. Overexpression of both catalytically-active and -inactive cathepsin D by cancer cells enhances apoptosis-dependent chemosensitivity. Oncogene 25, 1967–1973.

Berg, K., Puntervoll, P., Valdersnes, S., Goksøyr, A., 2010. Responses in the brain proteome of Atlantic cod (*Gadus morhua*) exposed to methylmercury. Aquatic Toxicology 100 (1), 51–65.

Bonifati, V., Rizzu, P., van Baren, M.J., Schaap, O., Breedveld, G.J., Krieger, E., Dekker, M.C., Squitieri, F., Ibanez, P., Joosse, M., van Dongen, J.W., Vanacore, N., van Swieten, J.C., Brice, A., Meco, G., van Duijn, C.M., Oostra, B.A., Heutink, P., 2003. Mutations in the DJ-1 gene associated with autosomal recessive early-onset parkinsonism. Science 299 (5604), 256–259.

Cardellichio, N., Decataldo, A., Di Leo, A., Misino, A., 2002. Accumulation and tissue distribution of mercury and selenium in striped dolphins (*Stenella coeruleoalba*) from the Mediterranean Sea (southern Italy). Environmental Pollution 116 (2), 265–271.

Castoldi, A.F., Coccini, T., Ceccatelli, S., Manzo, L., 2001. Neurotoxicity and molecular effects of methylmercury. Brain Research Bulletin 55 (2), 197–203.

Cookson, M.R., 2003. Pathways to parkinsonism. Neuron 37 (1), 7–10.

Crump, K.L., Trudeau, V.L., 2009. Mercury-induced reproductive impairment in fish. Environmental Toxicology and Chemistry 28 (5), 895–907.

Denslow, N.D., Garcia-Reyero, N., Barber, D.S., 2007. Fish 'n' chips: the use of microarrays for aquatic toxicology. Molecular BioSystems 3 (3), 172–177.

Dieguez-Acuña, F.J., Ellis, M.E., Kushleika, J., Woods, J.S., 2001. Mercuric ion attenuates nuclear factor-kappaB activation and DNA binding in normal rat kidney epithelial cells: implications for mercury-induced nephrotoxicity. Toxicology and Applied Pharmacology 173 (3), 176–187.

Dong, W.R., Xiang, L.X., Shao, J.Z., 2007. Cloning and characterisation of two natural killer enhancing factor genes (NKEF-A and NKEF-B) in pufferfish, *Tetraodon nigroviridis*. Fish and Shellfish Immunology 22 (1–2), 1–15.

Dutczak, W.J., Ballatori, N., 1994. Transport of the glutathionemethylmercury complex across liver canalicular membranes on reduced glutathione carriers. Journal of Biological Chemistry 269 (13), 9746–9751.

Frodello, J.P., Roméo, M., Viale, D., 2000. Distribution of mercury in the organs and tissues of five toothed-whale species of the Mediterranean. Environmental Pollution 108 (3), 447–452.

Giari, L., Simoni, E., Manera, M., Dezfuli, B.S., 2008. Histo-cytological responses of *Dicentrarchus labrax* (L.) following mercury exposure. Ecotoxicology and Environment Safety 70 (3), 400–410.

Görg, A., Obermaier, C., Boguth, G., Csordas, A., Diaz, J.-J., Madjar, J.-J., 1997. Very alkaline immobilized pH gradients for two-dimensional electrophoresis of ribosomal and nuclear proteins. Electrophoresis 18 (3–4), 328–337.

Gündel, U., Kalkhof, S., Zitzkat, D., Bergen, M., Altenburger, R., Küster, E., 2012. Concentration–response concept in ecotoxicoproteomics: effect of different phenanthrene concentrations to the zebrafish (*Danio rerio*) embryo proteome. Ecotoxicology and Environment Safety 76 (2), 11–22.

Hayes, J.D., McLellan, L.I., 1999. Glutathione and glutathione dependent enzymes represent a co-ordinately regulated defence against oxidative stress. Free Radical Research 31 (4), 273–300.

He, M., Rutledge, S.L., Kelly, D.R., Palmer, C.A., Murdoch, G., Majumder, N., Nicholls, R.D., Pei, Z., Watkins, P.A., Vockley, J., 2007. A new genetic disorder in mitochondrial fatty acid β-oxidation: ACAD9 deficiency. American Journal of Human Genetics 81 (1), 87–103.

Hoffmann, W., 1992. Goldfish ependymins: cerebrospinal fluid proteins of meningeal origin. Progress in Brain Research 91, 13–17.

Ibarz, A., Martín-Pérez, M., Blasco, J., Bellido, D., de Oliveira, E., Fernández-Borràs, J., 2010. Gilthead sea bream liver proteome at low temperatures by oxidative stress. Proteomics 10 (5), 963–975.

Joseph, P., Muchnok, T.K., Klishis, M.L., Roberts, J.R., Antonini, J.M., Whong, W.-Z., Ong, T.-M., 2001. Cadmium-induced cell transformation and tumorigenesis are associated with transcriptional activation of c-*fos*, c-*jun*, and c-*myc* proto-oncogenes: role of cellular calcium and reactive oxygen species. Toxicological Sciences 61 (2), 295–303.

Kagedal, K., Johansson, U., Ollinger, K., 2001. The lysosomal protease cathepsin D mediates apoptosis induced by oxidative stress. FASEB Journal 15 (9), 1592–1594.

Keyvanshokooh, S., Vaziri, B., Gharaei, A., Mahboudi, F., Esmaili-Sari, A., Shahriari-Moghadam, M., 2009. Proteome modifications of juvenile beluga (*Huso huso*) brain as an effect of dietary methylmercury. Comparative Biochemistry and Physiology Part D: Genomics and Proteomics 4 (4), 243–248.

Kim, S.H., Bark, H., Choi, C.H., 2005. Mercury induces multidrug resistance-associated protein gene through p38 mitogen-activated protein kinase. Toxicology Letters 155 (1), 143–150.

Königstorfer, A., Sterrer, S., Hoffmann, W., 1989. Biosynthesis of ependymins from goldfish brain. Journal of Biological Chemistry 264 (23), 13689–13692.

Kudo, A., Fujikawa, Y., Miyahara, S., Zheng, J., Takigami, H., Sugahara, M., Muramatsu, T., 1998. Lessons from minamata mercury pollution. Japan – after a continuous 22 years of observation. Water Science and Technology 38 (7), 187–193.

Leyva, J.A., Bianchet, M.A., Amzel, L.M., 2003. Understanding ATP synthesis: structure and mechanism of the F1-ATPase (review). Molecular Membrane Biology 20 (1), 27–33.

Li, H.M., Taira, T., Maita, C., Ariga, H., Iguchi-Ariga, S.M.M., 2006. Protection against nonylphenol-induced cell death by DJ-1 in cultured Japanese medaka (*Oryzias latipes*) cells. Toxicology 228 (2-3), 229–238.

Li, P., Feng, X.B., Qiu, G.L., Shang, L.H., Li, Z.G., 2009. Mercury pollution in Asia: a review of the contaminated sites. Journal of Hazardous Materials 168 (2–3), 591–601.

Looi, M.L., Karsani, S.A., Abdul Rahman, M., Mohd Dali, A.Z.H., Md Ali, S.A., Wan Ngah, W.Z., Mohd Yusof, Y.A., 2009. Plasma proteome analysis of cervical intraepithelial neoplasia and cervical squamous cell carcinoma. Journal of Biosciences 34 (6), 917–925.

Maki, A., Berezesky, I.K., Fargnoli, J., Holbrrok, N.J., Trump, B.F., 1992. Role of $(Ca^{2+})i$ in induction of c-*fos*, c-*jun*, and c-*myc* mRNA in rat PTE after oxidative stress. FASEB Journal 6 (3), 919–924.

McDonough, M.A., Kavanagh, K.L., Butler, D., Searls, T., Oppermann, U., Schofield, C.J., 2005. Structure of human phytanoyl-CoA 2-hydroxylase identifies molecular mechanisms of Refsum disease. Journal of Biological Chemistry 280 (49), 41101–41110.

Merrick, B.A., 2006. Toxicoproteomics in liver injury and inflammation. Annals of the New York Academy of Sciences 1076, 707–717.

Monteiro, D.A., Rantin, F.T., Kalinin, A.L., 2010. Inorganic mercury exposure: toxicological effects, oxidative stress biomarkers and bioaccumulation in the tropical freshwater fish matrinxã, *Brycon amazonicus* (Spix and Agassiz, 1829). Ecotoxicology 19 (1), 105–123.

Morel, F.M.M., Kraepiel, A.M.L., Amyot, M., 1998. The chemical cycle and bioaccumulation of mercury. Annual Review of Ecology and Systematics 29, 543–566.

Newton, B.W., Russell, W.K., Russell, D.H., Ramaiah, S.K., Jayaraman, A., 2009. Liver proteome analysis in a rodent model of alcoholic steatosis. Journal of Proteome Research 8 (4), 1663–1671.

Nøstbakken, O.J., Martin, S.A., Cash, P., Torstensen, B.E., Amlund, H., Olsvik, P.A., 2012. Dietary methylmercury alters the proteome in Atlantic salmon (*Salmo salar*) kidney. Aquatic Toxicology 108, 70–77.

Pan, K., Wang, W.X., 2011. Mercury accumulation in marine bivalves: influences of biodynamics and feeding niche. Environmental Pollution 159 (10), 2500–2506.

Pfeiffer, W.C., Lacerda, L.D., 1988. Mercury inputs in the Amazon region, Brazil. Environmental Technology Letters 9, 325–330.

Radyuk, S.N., Klichko, V.I., Spinola, B., Sohal, R.S., Orr, W.C., 2001. The peroxiredoxin gene family in *Drosophila melanogaster*. Free Radical Biology and Medicine 31 (9), 1090–1100.

Samikkannu, T., Chen, C.H., Yih, L.H., Wang, A.S., Lin, S.Y., Chen, T.C., Jan, K.Y., 2003. Reactive oxygen species are involved in arsenic trioxide inhibition of pyruvate dehydrogenase activity. Chemical Research in Toxicology 16 (3), 409–414.

Schaffeld, M., Schultess, J., 2006. Genes coding for intermediate filament proteins closely related to the hagfish thread keratins (TK) alpha and gamma also exist in lamprey, teleosts and amphibians. Experimental Cell Research 312 (9), 1447–1462.

Sheikh, A.M., Li, X., Wen, G., Tauqeer, Z., Brown, W.T., Malik, M., 2010. Cathepsin D and apoptosis related proteins are elevated in the brain of autistic subjects. Neuroscience 165 (2), 363–370.

Shen, L., Liu, Q., Ni, J., Hong, G., 2009. A proteomic investigation into the human cervical cancer cell line Hela treated with dicitratoytterbium (III) complex. Chemico-Biological Interactions 181 (3), 455–462.

Sørmo, E.G., Ciesielski, T.M., Øverjordet, I.B., Lierhagen, S., Eggen, G.S., Berg, T., Jenssen, B.M., 2011. Selenium moderates mercury toxicity in free-ranging freshwater fish. Environmental Science and Technology 45 (15), 6561–6566.

Stacchiotti, A., Morandini, F., Bettoni, F., Schena, I., Lavazza, A., Grigolato, P.G., Apostoli, P., Rezzani, R., Aleo, M.F., 2009. Stress proteins and oxidative damage in a renal derived cell line exposed to inorganic mercury and lead. Toxicology 264 (3), 215–224.

Tang, S.J., Sun, K.H., Sun, G.H., Lin, G., Lin, W.W., Chuang, M.J., 1999. Cold-induced ependymin expression in zebrafish and carp brain: implications for cold acclimation. FEBS Letters 459 (1), 95–99.

Torres, A.M., Dnyanmote, A.V., Bush, K.T., Wu, W., Nigam, S.K., 2011. Deletion of multispecific organic anion transporter Oat1/Slc22a6 protects against mercury-induced kidney injury. Journal of Biological Chemistry 286 (30), 26391–26395.

Toyama, T., Sumi, D., Shinkai, Y., Yasutake, A., Taguchi, K., Tong, K.I., Yamamoto, M., Kumagai, Y., 2007. Cytoprotective role of Nrf2/Keap1 system in methylmercury toxicity. Biochemical and Biophysical Research Communications 363 (3), 645–650.

Ung, C.Y., Lam, S.H., Hlaing, M.M., Winata, C.L., Korzh, S., Mathavan, S., Gong, Z., 2010. Mercury-induced hepatotoxicity in zebrafish: in vivo mechanistic insights from transcriptome analysis, phenotype anchoring and targeted gene expression validation. BMC Genomics 11, 212–227.

Volz, D.C., Hinton, D.E., Law, J.M., Kullman, S.W., 2006. Dynamic gene expression changes precede dioxin-induced liver pathogenesis in medaka fish. Toxicological Sciences 89 (2), 524–534.

Wang, J., Wang, Y.Y., Lin, L., Gao, Y., Hong, H.S., Wang, D.Z., 2012. Quantitative proteomic analysis of okadaic acid treated mouse small intestine reveals differentially expressed proteins involved in diarrhetic shellfish poisoning. Journal of Proteomics 75 (7), 2038–2052.

Wang, M.H., Chan, L.L., Si, M.Z., Hong, H.S., Wang, D.Z., 2010. Proteomic analysis of hepatic tissue of zebrafish (*Danio rerio*) experimentally exposed to chronic microcystin-LR. Toxicological Sciences 113 (1), 60–69.

Wang, M.H., Wang, Y.Y., Wang, J., Lin, L., Hong, H.S., Wang, D.Z., 2011. Proteome profiles in medaka (*Oryzias melastigma*) liver and brain experimentally exposed to acute inorganic mercury. Aquatic Toxicology 103 (3–4), 129–139.

Wiche, G., 1998. Role of plectin in cytoskeleton organization and dynamics. Journal of Cell Science 111 (Pt 17), 2477–2486.

Zalups, R.K., 2000. Molecular interactions with mercury in the kidney. Pharmacological Reviews 52 (1), 113–143.